CFD Simulation of Disc Radius and Blade Height Effects on Mixing Performance in the Unbaffled Tank Covered by a Lid

Awanee Wongnui   Charkorn Akavipat   Eakarach Bumrungthaichaichan   Santi Wattananusorn

Department of Chemical Engineering, Faculty of Engineering,
King Mongkut's Institute of Technology Ladkrabang

Abstract

The stirred tank is a general device in mixing processes. The aim of this work is to investigate the effect of disc radius and blade height on mixing performance by using CFD technique. The preliminary simulated results were validated by comparing with experimental data. The simulated results revealed that the shortest mixing time, which is depended on impeller geometry, average velocities, and ratio of k/ε, and minimum power can be achieved by 1b-disc3/4 (10.72 seconds) and 1b-disc1 (0.4892 watts), respectively. In order to investigate the correct optimal stirred tank, the mixing energy was conducted because the mixing time and power are combined into single parameter. In view of mixing energy, the optimal stirred tank was 1b-disc3/4 because of its lowest energy.

Keywords: CFD, Unbaffled Tank, disc radius, blade height

1. Introduction

Stirred tanks are commonly used in various chemical and process industries, such as liquid–liquid contactors, particle and droplet suspensions, polymer reactors, etc. Generally, the different types of baffle are adopted to achieve the well mixing. However, vessels without baffles are also used in many applications, such as crystallization, precipitation, solid–liquid mass transfer, solid suspension, in the food and dairy, etc.

Nowadays, the computational fluid dynamics (CFD) simulation has been widely applied in many applications. For mixing tank simulations, the results, e.g. velocity profile, power number, etc., are validated by comparing with the data obtained by laser doppler velocimetry (LDV) or particle image velocimetry (PIV)[1] to confirm the model.

Ochieng et al. [2] presented the effect of the impeller clearance on the velocity field and mixing. It has been shown that the Rushton turbine with low impeller clearance generates a flow field that evolves from the typical two loops to a single loop flow pattern similar to an axial impeller. This single loop flow pattern was increased axial flow and decreased mixing time at a constant power number.

Ameur et al. [3] investigated the effect of the curvature blade. The simulated results showed that the eddy is found to decrease with increasing the curvature blade. In order to reduce the mixing power, it is recommended to use a curved blade but the excessive increase in the blade curvature can reduce the cavern size. Therefore a very deep hollow blade is not required due to the blockage of fluid flow by the curved blade.

Alcamo et al.[4] used Large Eddy Simulation of turbulent flow in an unbaffled stirred tank covered by a lid and validated with the experimental data on the flow field of Vella et al.[5]. The results of the radial profiles of the tangential velocity of the experiment and LES were in excellent agreement.

Akavipat. [6] presented the effect of numbers of blade orifice on mixing performance. The simulated results of full tank and 1/6 tank were identical. The calculation time of 1/6 tank was lower than full tank simulation.

This research investigates the effect of disc radius and blade height on mixing performance by using ANSYS FLUENT®CFD software. The multiple reference frame (MRF) impeller model and Renormalization group k-epsilon (RNGKE) model were used to compute the turbulent field and mixing time.

2. Governing equations

The simulation was distinguished into two parts. First, the three-dimensional steady flow with constant kinematic viscosity was

simulated to obtain the velocity field. The turbulence was simulated by RNGKE. Then, the three-dimensional unsteady flow was computed to achieve the tracer concentration distribution by using species transport equation.

The general form of Reynolds average equations for mass, momentum, k-transport, ε-transport, and species transport equations can be written in the following compact form as shown in Eq. (1).

$$\frac{\partial(\rho\phi)}{\partial t} + \frac{\partial(\rho\overline{U}\phi)}{\partial x_i} = \frac{\partial}{\partial x_i}\left[\Gamma_\varphi \frac{\partial\phi}{\partial x_i}\right] + S_\varphi \quad (1)$$

where ϕ is a universal dependent variable, $\overline{U}$ is mean velocity vector, Γ_φ is the diffusivity, and S_φ is the source term. The details of variable for these equations are given in Table 1. Further, the model constants of RNGKE are given in Table 2.

3. Numerical method

The geometry of the investigated six-blade Rushton turbine with unbaffled tank covered by a lid is shown in Fig 1.The flat lid was employed to prevent central vortex formation. The tank diameter (T)was 0.19 m, the rotating shaft diameter was 0.0173 m, and the other details are given in Table 3.The disc diameter and blade height for this study are summarized in Table 4. In this research, the model of 1/6 tanks and their grid generations were done by using GAMBIT® [6].

The fluid is a pure water. The density and dynamic viscosity of water were 1,000 kg/m³

and 0.001 Pa·s, respectively. The properties of water and tracer were identical. The rotating speed of the impeller (N) was 200 rpm [4]. The wall boundary condition was no-slip.
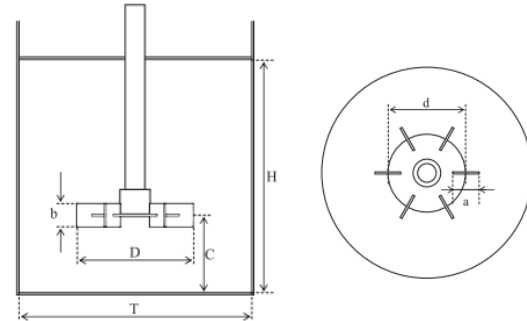

Fig 1. Geometry of the investigated tank

Table 2 Model constants for RNGKE model

$C_{1\varepsilon}$	$C_{2\varepsilon}$	C_μ
1.42	1.68	0.0845

Table 3 The standard geometry of the tank

H/T	D/T	C/T	a/D	b/D	d/D
1	1/2	1/3	1/4	1/5	3/4

Table 4 Simulation tests

d/D	Blade height (b)	
	1b	2b
5/8	1b-disc5/8	2b-disc5/8
3/4	1b-disc3/4[a]	2b-disc3/4
7/8	1b-disc7/8	2b-disc7/8
1	1b-disc1	2b-disc1

[a] Standard tank

Table 1 The details of variables for governing equations

Equation	ϕ	Γ_φ	S_φ
Continuity equation	1	0	0
Momentum equation	$\overline{u}$	μ	$-\dfrac{\partial\overline{p}}{\partial x_i} + \dfrac{\partial}{\partial x_i}\left[\mu_i \dfrac{\partial\overline{u}_i}{\partial x_i}\right] + S_{M,i}$
k-transport equation	k	$\alpha_k(\mu+\mu_t)$	$G_k + G_b + \rho\varepsilon - Y_M + S_k$
ε-transport equation	ε	$\alpha_\varepsilon(\mu+\mu_t)$	$C_{1\varepsilon}\dfrac{\varepsilon}{k}(G_k + C_{3\varepsilon}G_b) - C_{2\varepsilon}\rho\dfrac{\varepsilon^2}{k} - R_\varepsilon + S_\varepsilon$
Species transport equation	Y_i	-	$-\dfrac{\partial\overline{J}_i}{\partial x_i} + R_i + S_i$

Governing equations were solved numerically by using ANSYS FLUENT®. The turbulence model is RNGKE. The impeller rotation was modelled by using the MRF impeller model. The pressure-velocity coupling of this simulation was SIMPLEC algorithm. The spatial discretization of gradient and pressure were Green-Gauss cell based and body force weighted, respectively. The second order upwind scheme was applied to calculate momentum, turbulence kinetic energy and turbulence dissipation rate.

4. Results and discussions

4.1 Model validation

The 1/6 standard tank with 697,449 hexahedral cells was validated by comparing with the experiment [5]. This used grid generation, which obtained by two times wall boundary adaption and two times moving zone adaption, was grid independent solutions.
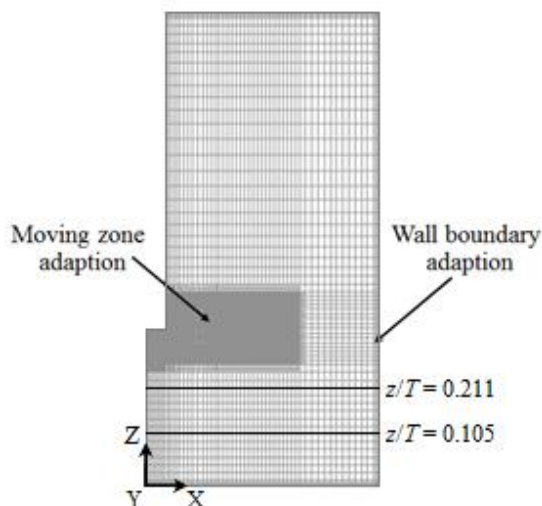

Fig. 2 Grid generation of validated model

The simulated tangential velocity profiles along the radial position for two different height were validated by comparing with the experimental data [5].The normalized tangential velocity was defined as the ratio of tangential velocity to tip velocity. Further, the normalized radial position was a ratio of radial position to tank radius. The simulated normalize tangential velocity profiles for z/T of 0.105 and 0.211 shown in Fig. 3.

In Fig. 3, at $r/R < 0.5$, the normalized tangential velocity profiles for two different z/T are found to increase with increasing r/R.
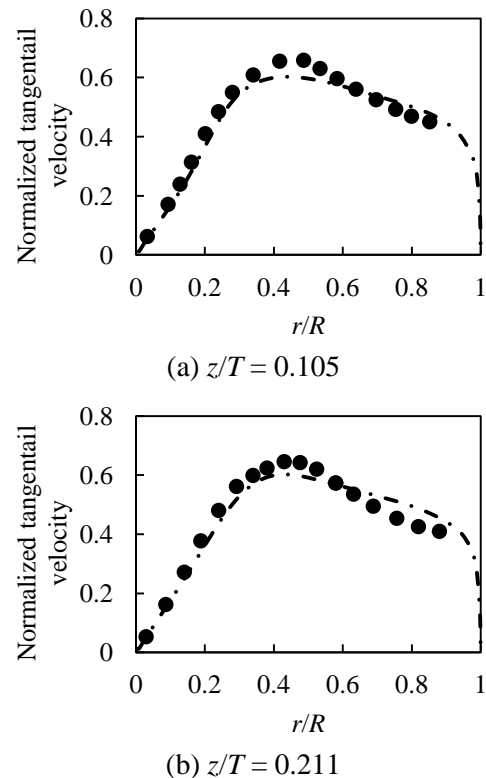

(a) $z/T = 0.105$

(b) $z/T = 0.211$

Fig. 3 Radial profiles of tangential velocity at different heights: ● Experiment; — · — CFD

Then, the normalized tangential velocity profiles are decreased with increase in r/R. Further, the predicted results are slightly different as compared to the experiment. Hence, it can be concluded that the simulation results were in good agreement with experiment. In other words, this model can be predicted the mixing tank agitated by Rushton turbine.

Hence, the simulation setup of 7 other stirred tanks as depicted in Table 4 were similar to the validation case setup. In this study, the mixing time and power were employed to investigate the optimal mixing tank.

4.2 Mixing time

In this part, the unsteady state of species transport equation was adopted to obtain the tracer concentration profiles. The tracer was injected at 5 mm above the center of the bottom tank. The tracer concentration profiles were measured at 6 different probe locations as shown in Table 5. The concentration profile was reported in dimensionless form, which can be defined as the ratio of the local tracer concentration to well mixed

concentration. The mixing time can be obtain from the time which concentration at any point in the tank has reached 95% as shown in Eq. (2).The normalized tracer concentration of standard tank (1b-disc3/4) is shown in Fig. 4.

$$t_{95\%} = \text{time for} \left| \frac{c - \bar{c}}{\bar{c}} \right| \le 0.05 \qquad (2)$$

Table 5 Locations of 6 probes

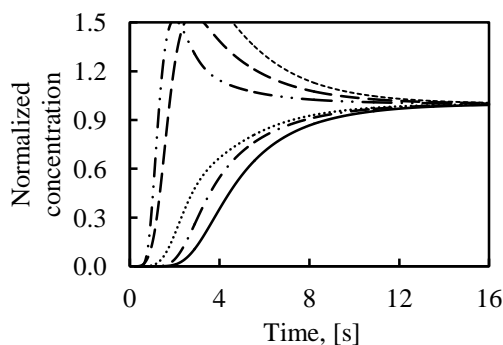| Probe	1	2	3	4	5	6
x	20	20	20	80	80	90
y	0	0	0	30	30	0
z	180	95	10	180	10	95

*** Unit in mm

Fig. 4 Normalized concentration of standard tank: —— Probe 1; ·········Probe 2; ------ Probe 3; –·– Probe 4; –– Probe 5; –··– Probe 6

In Fig. 4, the normalized concentration of standard tank for 6 different probes are different. Probe 6 and probe 3 show the shortest and longest mixing times, respectively. According to these results, the longest mixing time obtained by probe 3 was employed to indicate the mixing time of the tank. Further, the normalized concentration profiles of probe 3 were also used to examine the mixing time for other tanks. The mixing time for 8 tanks can be summarized as shown in Table 6.

In Table 6, for 1b tanks, the 1b-disc3/4 tank provides the shortest mixing time followed by 1b-disc1 tank, 1b-disc5/8 tank, and 1b-disc7/8 tank, respectively. These simulated results revealed that the mixing time of these tanks show no predictable tendency as the disc radius is increased. For 2b tanks, the shortest mixing time is occurred in 2b-disc5/8 tank followed by 2b-disc3/4 tank, 2b-disc7/8 tank, and 2b-disc1 tank, respectively. These results showed that the mixing time is increased with increasing the disc radius.

In order to elucidate the difference in mixing time, the average radial velocity (v_{radial}) and average axial velocity (v_{axial}) in moving zone were conducted as shown in Table 6. From Table 6, for 1b tanks, the highest average axial and average radial velocities are occurred in the 1b-disc3/4 tank follow by 1b-disc5/8 tank, 1b-disc7/8 tank, and 1b-disc1 tank, respectively. According to these results, as the disc radius is increased, the average velocities of these 1b tanks represent no predictable tendency, which is similar to the mixing time. In contrast, for 2b tanks, these average velocities are found to decrease with increasing the disc radius. According to these results, it can be seen that the mixing time of these 2b tanks are depended on the average radial and axial velocities, that is, the higher average velocities yield the shorter mixing time.

Table 6 The simulated mixing time, average velocities, and turbulent quantities of 8 different tanks

Tank	Mixing time (s)	Average velocities in moving zone		k $(10^{-2}\,m^2/s^2)$	ε $(10^{-2}\,m^2/s^3)$	k / ε (s)
		v_{Radial} $(10^{-2}\,m/s)$	v_{Axial} $(10^{-2}\,m/s)$			
1b-disc5/8	11.29	9.606	-0.754	1.116	9.227	0.121
1b-disc3/4	10.72	9.633	-0.833	1.128	9.225	0.122
1b-disc7/8	11.50	9.521	-0.385	1.098	9.064	0.121
1b-disc1	11.25	9.167	-0.008	1.049	8.948	0.117
2b-disc5/8	10.84	5.889	-3.679	1.489	11.210	0.133
2b-disc3/4	10.90	5.847	-1.362	1.453	10.987	0.132
2b-disc7/8	11.05	5.844	-1.060	1.428	10.845	0.132
2b-disc1	11.57	5.784	-0.932	1.409	10.769	0.131

Moreover, for 1b tanks, only average radial and axial velocities were not sufficient to describe the irregular tendency of the mixing time. Hence, the turbulence quantities were also adopted to indicate this irregular tendency of the mixing time. In this work, the turbulence quantities were defined as a ratio of turbulent kinetic energy (k) to its dissipation rate (ε). This ratio represents the mixing ability due to small turbulence scale. Further, this ratio can be interpreted as the efficiency of turbulent kinetic energy usability. If the turbulent kinetic energy in two tanks are identical, the tank with the higher value of turbulent dissipation rate yields the shorter mixing time because the trans-formation of large turbulence scale to small scale is faster than another tank. Hence, the smaller value of k/ε provides the shorter mixing time. This ratio of 8 different tanks are shown in Table 6.

From Table 6, for 1b tanks, it can be seen that the 1b-disc1 tank illustrates the lowest value of k/ε. Moreover, the value of k/ε of 1b-disc5/8 and 1b-disc7/8 tanks are identical. The highest value of k/ε is occurred in the 1-disc3/4 tank. The lowest value of k/ε in 1b-disc1 can be reduced the mixing time while the average axial and radial velocities show the lowest value because the transformation of turbulence scale is faster than other tanks. However, the mixing time of 1b-disc3/4 is the minimum because of the highest values of average axial and radial velocities. According to these results, it can be implied that the mixing time of 1b tank is not only depended on average velocities but also the ratio of k/ε. In contrast, for 2b tanks, the values of k/ε for 4 different tanks are slightly different. Thus, it can be concluded that the mixing times of 2b tanks are only depended on average velocities.

However, only mixing time is not sufficient to indicate the optimal stirred tank. Thus, the power and energy should be integrated to consider the optimal mixing tank.

4.3 Power and energy

In order to obtain the required power, the predicted torque was conducted. The predicted power (P) can be calculated by using the relation as shown in Eq. (3). Moreover, the energy, which is used to obtain the mixing in the tank, is determined by using Eq. (4).

$$P = \tau \times 2\pi \times N \qquad (3)$$

$$\text{Energy} = \text{Power x Mixing time} \qquad (4)$$

where P is power (watt), τ is torque (N·m), π is radian, N is impeller speed (rps), and unit of energy is N·m (J).The predicted power and energy of 8 tanks are shown in Table 9.

In Table 9, it can be seen that the 1b-disc1 and 2b-disc1 tanks show the minimum predicted power for the blade height of 1b and 2b, respectively. The maximum power for the blade height of 1b and 2b are 1b-disc5/8 and 2b-disc5/8, respectively. The minimum predicted power obtained by 1b-disc1 tank is due to the smallest wake region behind the blade. Generally, the wake region is resulted in the pressure drag, that is, the smaller wake region yields smaller pressure drag. Hence, the smaller pressure drag leads to smaller power. For power viewpoint, the optimal stirred tank should be 1b-disc1 tank.

Table 9 Power and Energy of simulation tests

	Power (Watts)	Energy (N·m)
1b-disc5/8	0.5023	5.6720
1b-disc3/4	0.5006	5.3668
1b-disc7/8	0.4943	5.6860
1b-disc1	0.4892	5.5040
2b-disc5/8	0.5960	6.4630
2b-disc3/4	0.5869	6.3950
2b-disc7/8	0.5770	6.3772
2b-disc1	0.5735	6.6369

When mixing time in Table 6 and power in Table 9 are viewed together, the shortest mixing time and minimum power are 1b-disc3/4 and 1b-disc1 tanks, respectively. In order to investigate the correct optimal stirred tank, the mixing energy should be conducted. Because the mixing time and power are combine into a single parameter. In other words, the mixing energy represents the mixing time and power at once. The energy for 8 different tanks are also represented in Table 9.

In Table 9, it can be seen that the minimum energy can be obtained by 1b-disc3/4 tank. This minimum energy was due to the minimum mixing time.

According to these results, it can be concluded that the 1b-disc3/4 was the optimal stirred tank in this study. Moreover, the suitable parameter which indicates the optimal mixing tank was the energy.

5. Conclusion

In this work, the effect of disc radius and blade height on mixing performance were investigated by using FLUENT®. The MRF with RNGKE model were used to compute the turbulent field and mixing time in 1/6 tank. The predicted results were validated by comparing with experiment [5]. The preliminary results were in good agreement with experimental data.

In this study, the simulated results revealed that the mixing time is depended on impeller geometry, average axial velocity, average radial velocity, and the ratio of k/ε.

The optimal stirred tank was considered by using energy. The simulated results showed that the 1b-disc3/4 exhibits the smallest energy as compared to the other tanks.

According to these results, it can be concluded that the optimal stirred tank was 1b-disc3/4 because of its lowest energy. Further, the energy was an important parameter to indicate the optimal mixing tank because the mixing time and power were considered together.

6. Nomenclature

6.1 Alphabetical Symbols

G_b	The generation of turbulence due to buoyancy
G_k	The production of turbulence kinetic energy
$\overline{J_i}$	Diffusion flux of species i
k	Turbulent kinetic energy, $m^2 \cdot s^{-2}$
$\bar{p}$	Mean pressure, Pa
R_i	Net rate of production of species i by chemical reaction
S_i	Species source term
S_k	Turbulent kinetic energy source term
S_M	Momentum source term
S_ε	Dissipation rate of turbulent kinetic energy source term
S_φ	Source term
Y_i	Mass fraction of species i
Y_M	Dilatation dissipation term
c	Concentration, $mol \cdot L^{-1}$
$\bar{c}$	Fully mixed concentration, $mol \cdot L^{-1}$
$\overline{U}$	Mean velocity vector, $m \cdot s^{-1}$
P	Power, watt
N	Impeller speed, rps

6.2 Greek Symbols

ε	Dissipation rate of turbulent kinetic energy, $m^2 \cdot s^{-3}$
μ	Fluid Viscosity, Pa·s
μ_t	Turbulent viscosity, Pa·s
ρ	Fluid density, $kg \cdot m^{-3}$
τ	Stress tensor, N·m
$\alpha_k, \alpha_\varepsilon$	Inverse effective Prandtl number for k and ε
ϕ	Universal dependent variable
Γ_φ	Diffusivity
π	Radian

7. Acknowledgement

8. References

[1] T. Yoshizawa, Handbook of Optical Metrology: Principles and Applications, Taylor& Francis Group, 2009

[2] A. Ochieng, M. S. Onyango, A. Kumar, K. Kiriamiti, and P. Musonge "Mixing in a tank stirred by a Rushton turbine at a low clearance",Chemical Engineering and Processing, vol. 47, No.5, pp.842–851, 2008

[3] H. Ameur and M. Bouzit "Numerical investigation of flow induced by a disc turbine in unbaffled stirred tank", Acta Scientiarum Technology, July-Sept, pp. 469-476, 2013

[4] R. Alcamo, G. Micale, F. Grisafi, A. Brucato, and M. Ciofalo "Large-eddy simulation of turbulent flow in an unbaffled stirred tank driven by a Rushton turbine", Journal of Chemical Engineering Science, vol.60, pp. 2303 – 2316, 2005

[5] C. Vella, F. Grisafi, G. Micale, L. Rizzuti,and A. Brucato, "Near impeller flow field in an unbaffled stirred tank", Proceedings of the 11th European Conference on Mixing, preprint VDI-GVD Bamberg, 14–17 October, pp. 629–636, 2003

[6] C. Akavipat, "Computational fluid dynamics study on effects of impeller Geometries on flow pattern in stirred tank," Master of Chemical Engineering Thesis, faculty of engineering King mongkut's institute of technology ladkrabang, 2014.